Journal of Power Sources 250 (2014) 166–173

Contents lists available at ScienceDirect

Journal of Power Sources

journal homepage: www.elsevier.com/locate/jpowsour

Long-term evaluation of solid oxide fuel cell candidate materials in a 3-cell generic short stack fixture, Part II: Sealing glass stability, microstructure and interfacial reactions

Yeong-Shyung Chou*, Jeffry W. Stevenson, Jung-Pyung Choi

K2-44, Energy and Efficiency Division, Pacific Northwest National Laboratory, P.O. Box 999, Richland, WA 99354, USA

HIGHLIGHTS

- A sealing glass was demonstrated chemically compatible with YSZ after 800 °C/6000 h.
- SEM showed some corrosion of alumina protection layer; however, no chromate was formed.
- Volatility study showed two stages of weight loss behavior.

ARTICLE INFO

Article history:
Received 24 June 2013
Received in revised form
25 September 2013
Accepted 29 September 2013
Available online 13 November 2013

Keywords:
Sealing glass
AISI441
Aluminization
(Mn, Co)-spinel
SOFC

ABSTRACT

A generic solid oxide fuel cell stack test fixture was developed to evaluate candidate materials and processing methods under realistic conditions. Part II of the work examined the sealing glass stability, microstructure development, interfacial reaction, and volatility issues of a 3-cell stack with LSM-based cells. After 6000 h of testing, the refractory sealing glass YSO7 showed desirable chemical compatibility with YSZ electrolyte in that no discernable interfacial reaction was identified. In addition, no glass penetration into the thin electrolyte was observed. At the aluminized AISI441 interface, the protective alumina coating appeared to be corroded by the sealing glass. Air side interactions appeared to be more severe than fuel side interactions. Metal species such as Cr, Mn, and Fe were detected in the glass, but were limited to the vicinity of the interface. No alkaline earth chromates were found at the air side. Volatility was also studied in a similar glass and weight loss in a wet reducing environment was determined. Using the steady-state volatility data, the life time weight loss of refractory sealing glass YSO77 was estimated to be less than 0.1 wt%.

© 2013 Published by Elsevier B.V.

1. Introduction

Solid oxide fuel cells (SOFCs) are an emerging technology which converts chemical energy directly to electrical energy at elevated temperatures. The energy conversion employs an ionic conductor (e.g., oxygen ion conductor such as YSZ) through which fuel and oxidant can react electrochemically, instead of through conventional combustion processes. Hence SOFCs can have higher energy conversion efficiency and a CO_2-concentrated exhaust which offers a more feasible and economic gas stream for carbon capture [1,2]. Stationary and transportational applications are current potential industrial markets. Two generic designs of SOFCs, tubular and planar, [3–5] are both being considered. For planar SOFCs, the advancement of ceramic processing has led to the development of the state-of-the-art anode-supported thin (<10 μm) electrolyte cells for which the operation temperatures can be lowered from ~1000 °C to ~800 °C. As a result, metals are being considered as potential interconnect materials, instead of the fragile and difficult-to-process ceramic interconnect such as $LaCrO_3$. However, great challenges are encountered when using metallic interconnect materials in a planar-type SOFCs where multiple tens of repeating unit cells are separated by metallic interconnect plates. These challenges apply to a spectrum of SOFC materials in terms of chemical compatibility, thermal stability, structural integrity, and electrical properties. For example, hermetic and durable sealing becomes more difficult when sealing dissimilar materials like metal to ceramic as compared to ceramic to ceramic, especially in the harsh dual environment with numerous thermal cycles and long life time requirements (e.g., ~40,000 h) at elevated temperatures. Chemical compatibility is another major concern for metallic interconnects when glass sealants are used. Current glass sealants,

* Corresponding author. Tel.: +1 509 375 2527; fax: +1 509 375 2186.
E-mail address: yeong-shyung.chou@pnnl.gov (Y.-S. Chou).

0378-7753/$ – see front matter © 2013 Published by Elsevier B.V.
http://dx.doi.org/10.1016/j.jpowsour.2013.09.148

such as a crystallizable glass like G18 which turns into a glass ceramic or a crystallization-resistant glass like the compliant SCN-1 glass, all contain appreciable amount of alkaline earths such as Ba and Sr [6–8]. These alkaline earths were found to be very reactive with Cr from metallic interconnects to form $BaCrO_4$ or $SrCrO_4$, whose very high thermal expansion can cause seal failure, if no protective coating is applied to the metal [9,10]. In addition to the chemical compatibility between sealing glass and Cr-containing metals, the issue of cathode poisoning is the primary concern when using these metals, as published in previous literature [11–16]. The coating not only needs to block Cr outward diffusion but also must be electrically conductive. A novel (Mn,Co)-spinel coating was therefore developed for ferritic stainless steels such as AISI441, which is a leading candidate for metallic interconnect as well as the window frame that surrounds the fragile ceramic cell [17,18]. These candidate materials have been extensively studied on their own or in small button-sized cells, but the behavior in a realistic SOFC stack environment, however, was rarely reported. It was therefore the objective of this work to study these candidate materials in a generic stack fixture to fully assess their stabilities and interactions with mating materials for long-term operation. Part one of the work reported the design of a generic stack fixture, cell assembly, seal system, and each cell's performance [19]. Part two of the work will address the sealing glass microstructure development, materials stability, and interfacial reactions with mating materials.

2. Experimental

2.1. Materials and stack fixture

A short stack of three cells was assembled using the generic stack test fixture. A schematic drawing of the assembly is shown in Fig. 1 [19]. A commercial NiO–YSZ anode supported thin YSZ electrolyte cell of 50 mm × 50 mm × 0.5 mm with LSM–YSZ composite cathode was used. The cells were sealed onto aluminized AISI441 window frames with refractory sealing glass YSO77 and stacked together with hybrid micas as the perimeter seal. LSM and NiO were used as cathode and anode contact materials, respectively. Ni mesh was also used at the anode side as a current collector while no metallic mesh was used at the cathode side. Ferritic stainless steel AISI441 was used to fabricate the interconnect plates and window frame, and was coated on the active cathode area with Ce-modified (Mn,Co)-spinel coating. The rest of the surface area was aluminized. The details of the cell, materials, coatings, processing and heat treatment are given in Ref. [19].

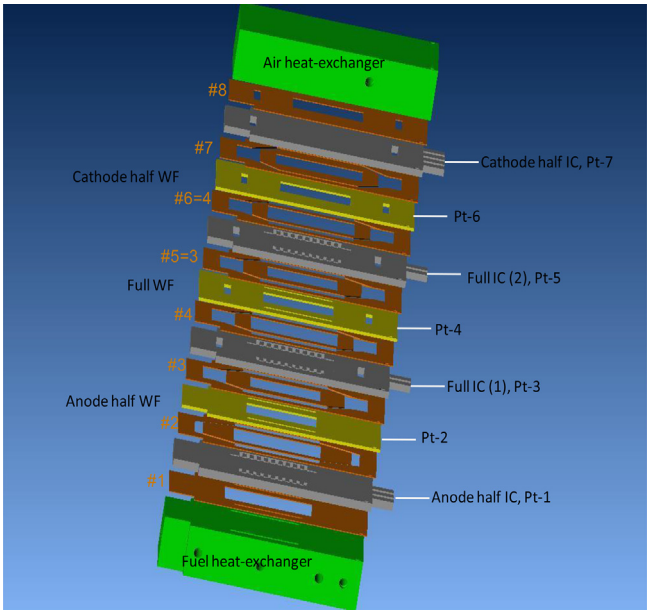

Fig. 1. Schematic drawing showing the assembly of the 3-cell short stack: three window frame plates in yellow, 4 interconnect plates in gray, 8 hybrid mica seals in brown. All were pressed between two heat exchangers for fuel and air, shown in green. WF = window frame, IC = interconnect, Pt = platinum wire (from Ref. [19]). (For interpretation of the references to color in this figure legend, the reader is referred to the web version of this article.)

2.2. Post-mortem characterization

After the long-term test, the short stack was dis-assembled. The post-mortem analysis was conducted with both optical microscopy and scanning electron microscopy with energy dispersion spectroscopy (JOEL SEM model 5900LV). Characterization with optical

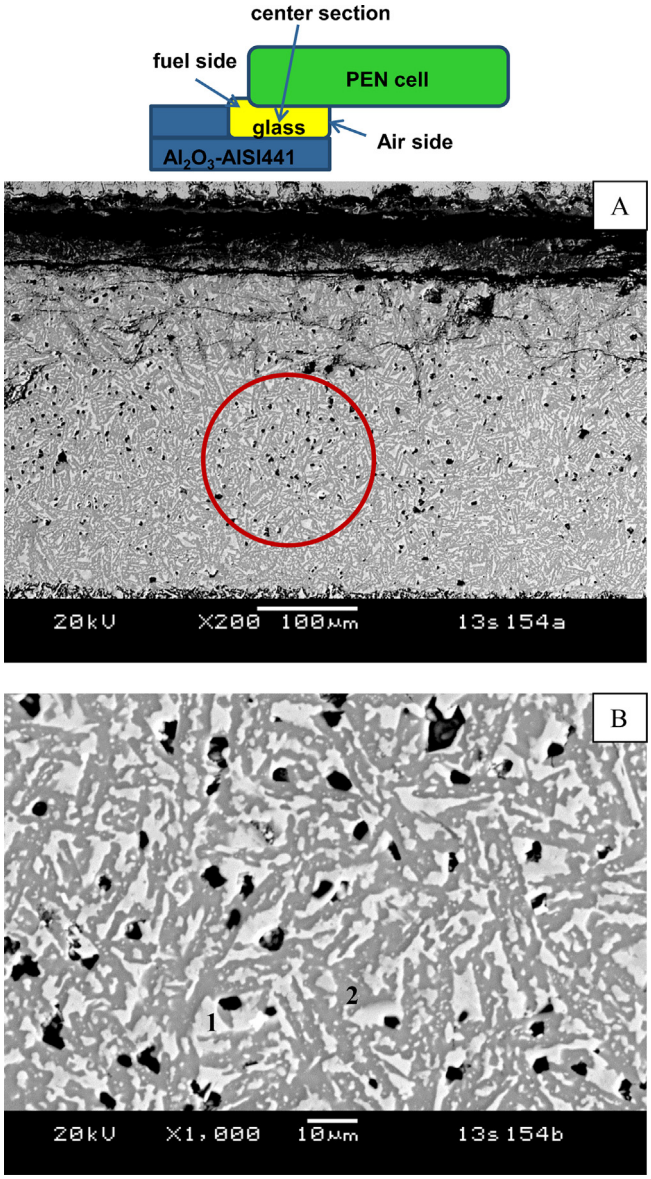

Fig. 2. Microstructure of the sealing glass YSO77 from the central section after 800 °C/6000 h test, (A) low magnification and (B) high magnification of the circled area in (A). The insert shows the location of glass for characterization. EDS of spots#1 and #2 are listed in Table 1.

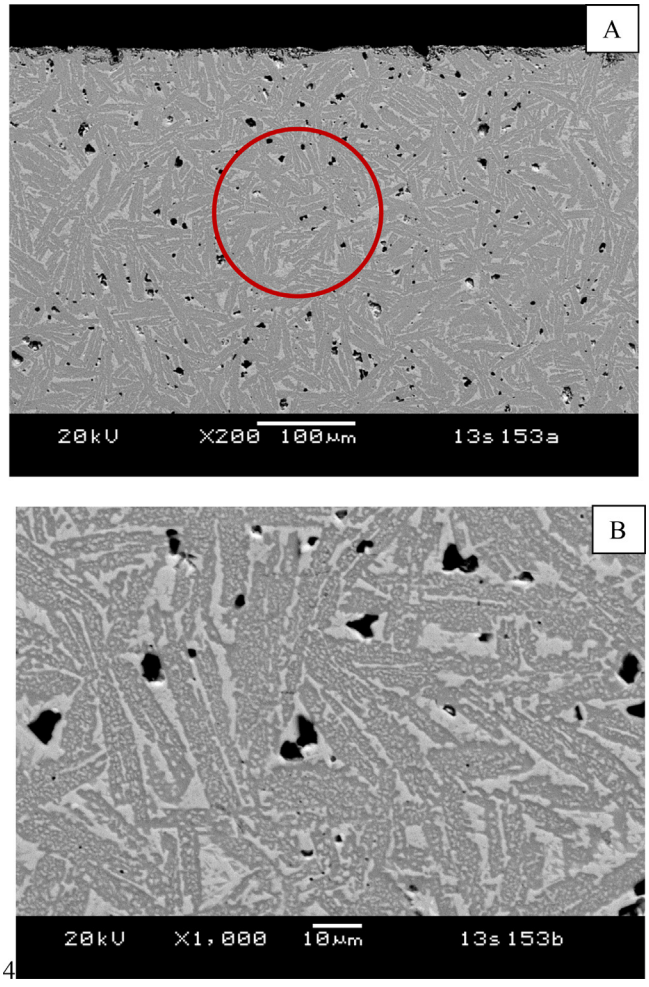

Fig. 3. Microstructure of the sealing glass YSO77 from the central section after 800 °C/896 h from another cell test for comparison, (A) low magnification and (B) high magnification of the circled area in (A).

microscopy, which was reported in Part one [19], showed that only the top cell remained hermetic during the entire test. The middle and the bottom cells experienced leakage during the course of operation. In Part two the materials' characterization was mostly focussed on the top cell and mating interconnect plates. The cell with the aluminized AISI441 window frame plate was first mounted with epoxy and then cut to smaller sizes. The samples were then remounted, ground, polished with typical metallurgical preparation, and coated with carbon for SEM analysis.

2.3. Volatility study

A volatility study was conducted on a similar glass, YSO75 (Sr–Ca–Y–B–Si), which had the same chemical composition as YSO77 (Sr–Ba–Y–B–Si), except for 6 mol% CaO instead of 6 mol% BaO. A sintered YSO75 sample was cut into a rectangular shape of ~20 mm × 10 mm × 3 mm and placed in a high-purity alumina tube furnace. A wet reducing gas was used to mimic the actual SOFC environment of high humidity. The reducing gas (2.75% H_2/Ar) at a flow rate of ~100–150 ml min^{-1} was first bubbled through a hot water bath set at 70 °C to take up ~30 vol.% H_2O, before entering the furnace. The temperature was set at 800 °C and the test was periodically stopped to measure the weight change.

Table 1
Chemical analysis of spots#1–#2 in Fig. 2B.

Spot#	O	Al	Si	Ca	Sr	Y	Ba
1	70.08	0.07	4.91	0.13	11.54	10.91	2.37
2	62.28	0.00	19.04	0.00	16.64	0.47	1.63

3. Results and discussion

3.1. Microstructure of the refractory sealing glass

A refractory-type sealing glass (YSO77) was used for the cell-to-aluminized AISI441 window frame seal which was fabricated at 930 °C 2 h prior to stack assembly. The choice of the crystallizing refractory glass YSO77 (Sr–Ca–Y–B–Si with small amount of Ba, 6%) was based on its matching CTE, potential good thermal stability similar to its parent glass YSO1 (Sr–Ca–Y–B–Si, contains no Ba), and likely chemical compatibility with the mating materials: YSZ and aluminized AISI441. Using these refractory type sealing glass may also enhance the bonding of contact materials, especially at the cathode side, since higher sealing temperatures can be used compared to alternative less-crystallizing sealing glasses (e.g., compliant sealing glass SCN-1). For example, the final firing of the

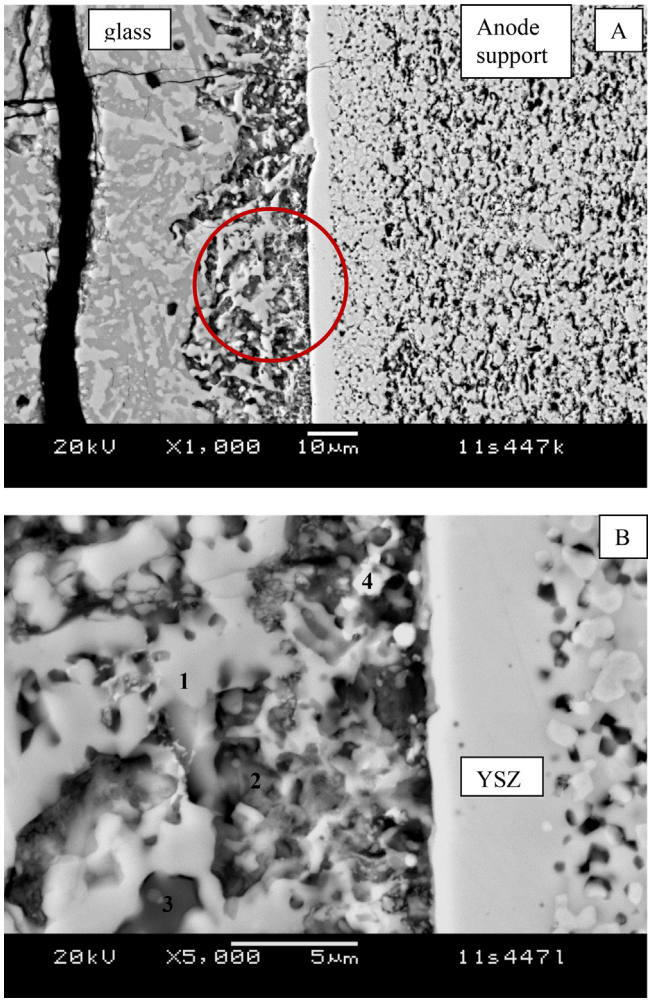

Fig. 4. Microstructure of the refractory sealing glass at the YSZ electrolyte interface near the air side, (A) low magnification shows the glass, YSZ dense electrolyte and the porous anode support, (B) higher magnification of the circled region in (A). The chemical analysis of spots (#1–#4 in B) is listed in Table 2.

stack assembly can reach ~950 °C while it should be kept below ~850 °C for compliant glass SCN-1. As a result, a typical cathode contact material such as LSM20 would achieve better bonding with the mating materials, i.e., LSM cathode of the cell and Ce-(Mn,Co)-spinel coating on the interconnect plate. A strong bonding is generally required for good electrical conduction and thermal cycle stability in SOFC's. In addition to the required chemical compatibility (as discussed below) with mating materials, the bulk sealing glass should also have good thermal stability and microstructure stability without substantial abnormal grain growth and large pore formation, as the presence of these defects could lead to seal failure during routine thermal cycling. Fig. 2 shows the microstructure of glass YSO77 from the central section (see the insert in the figure for the location) after the long-term 800 °C/6000 h test. For comparison, the glass microstructure from another single cell tested at the same condition but for a shorter period of time (800 °C/896 h) is also included in Fig. 3. Clearly no substantial abnormal grain growth or large pores were found. In addition, the pores appeared to be irregularly shaped, instead of circular (Figs. 2B and 3B). This is consistent with the behavior of the crystallizing refractory sealing glass, which tends to crystallize rapidly and have a much higher softening point afterward. For example, the dilatometric softening point for as-prepared YSO77 bulk glass was 703 °C, which increased to 884 °C after sintering a pressed powder compact at 950 °C for 2 h. With rigid crystalline phases present along with residual glassy phase, the mobility of pores was greatly reduced, and pore coarsening by coalescence of small pores was inhibited. The majority of the pores were less than 10 microns in size, with a few in the range of 20–30 microns. There were no discernable changes in pore size and distribution between 896 h and 6000 h, indicating the desired microstructure stability. Two phases were visible in the glass microstructure (Figs. 2B and 3B). The darker phase had a rod-shaped morphology of ~30–50 microns length and ~10 microns thickness, while the light phase was uniformly distributed between the dark phase grains without distinct morphology. EDS of these two phases (Fig. 2B) showed the dark phase was composed primarily of Sr, Ba and Si with (Sr,Ba)/Si ratio close to 1 (Table 1), suggesting (Sr,Ba)SiO_3. The white phase contained Sr, Y, Si, Ba, and traces of Ca and Al; however, no crystalline phase with similar atomic ratios could be identified. It is also interesting to note that the rod-shaped phases showed uniform and random distribution throughout the whole thickness, with no distinct difference in morphology and distribution near the interfaces. This suggests that the crystallization of the dark rod-shaped phases occurred via classical homogeneous nucleation and growth, instead of the surface dominated heterogeneous nucleation and growth. Although the microstructures of the 896 h and 6000 h samples were very similar overall, it appeared that the tiny white precipitates within each dark rod-shaped grain coalesced and coarsened during the 6000 h test.

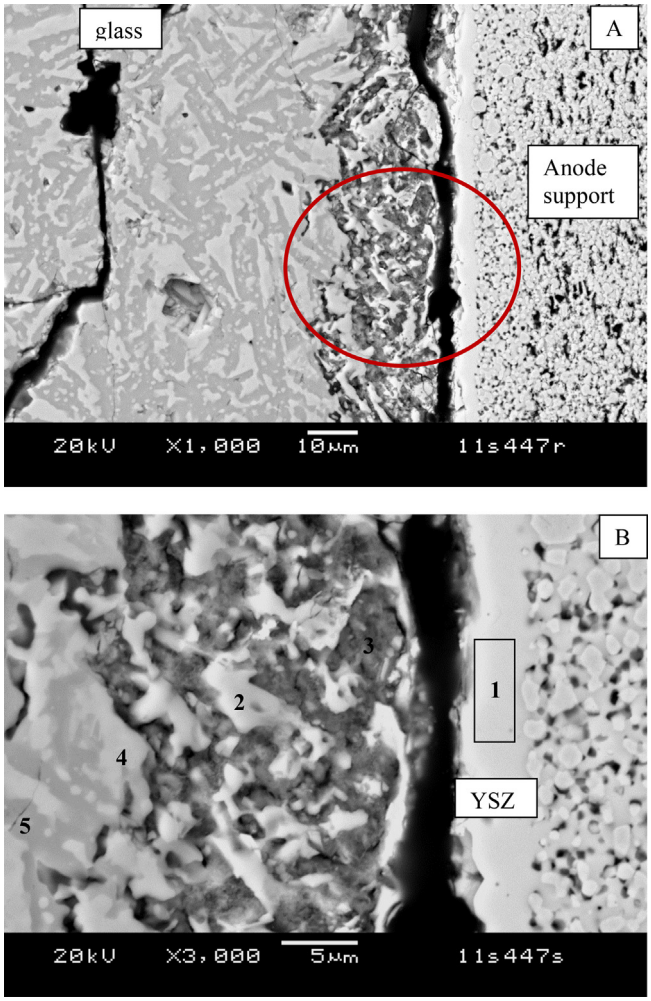

Fig. 5. Microstructure of the refractory sealing glass at the YSZ electrolyte interface near the fuel side, (A) low magnification shows the glass, YSZ dense electrolyte and the porous anode support, (B) higher magnification of the circled region in (A). The chemical analysis of spots (#1–#5 in B) is listed in Table 3.

3.2. Refractory sealing glass at YSZ electrolyte interface

As mentioned earlier, sealing glass YSO77 was derived from its parent glass YSO1, which was found to show good thermal stability without changes in crystalline phases and CTE, in both oxidizing and reducing environments for up to 2000 h at 900 °C [8]. The major crystalline phases were identified as $BaSiO_3$, $SrSiO_3$ and $BaAl_2Si_2O_8$ for these alkaline-earth containing Ba–Ca–Al–B–Si and Sr–Ca–Y–B–Si glasses [6,8]. Due to its rapid crystallization behavior, the glass was expected to have minimum reactivity with YSZ electrolyte, especially at the operation temperature of 800 °C. Simple thermodynamics calculation (using commercial software HSC v5.1 by Outokumpu, Finland) of potential reactions between major species (SrO, SiO_2, ZrO_2, and BaO) at 800 °C are listed below:

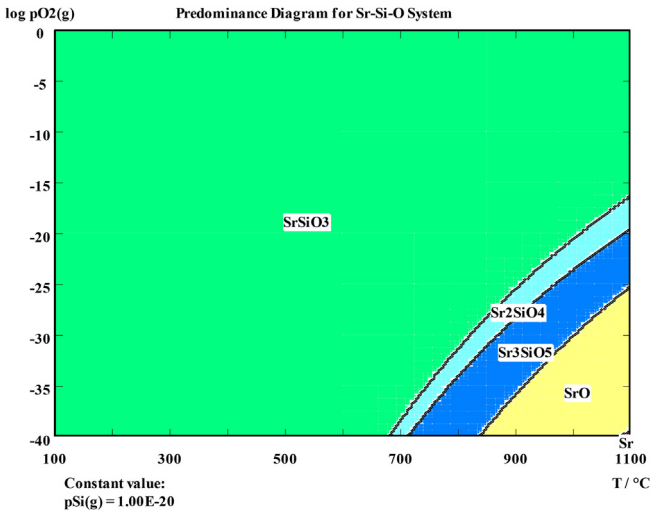

Fig. 6. Predominance diagram for Sr–Si–O as function of temperature and PO_2.

Table 2
Chemical analysis of spots#1–#4 in Fig. 4B.

Spot#	O	Mg	Al	Si	S	Ca	Fe	Ni	Cu	Sr	Y	Zr	Ba
1	71.07			4.14						11.89	10.32		2.57
2	67.62	1.15	0.65	10.55	1.71	0.88	0.29			8.54	3.42		5.20
3	66.10	0.57		17.91		0.40				7.40	4.89		2.73
4	76.26			3.94		0.26		0.28	0.37	6.65	4.80	4.43	3.00

Table 3
Chemical analysis of spots#1–#5 in Fig. 5B.

Spot#	O	Mg	Si	S	Ca	Fe	Ni	Sr	Y	Zr	Ba
1	69.52						0.65		4.98	24.85	
2	66.68		9.43					10.59	11.70		1.60
3	58.80	2.09	16.77	2.18	2.25		0.40	7.68	4.56		5.27
4	68.81		5.04			0.40		12.37	10.35		3.03
5	62.27		18.94					15.93	1.37		1.49

$$SrO + SiO_2 = SrSiO_3,\ \Delta G = -132\ \text{kJ mol}^{-1} \quad (1)$$

$$BaO + SiO_2 = BaSiO_3,\ \Delta G = -161\ \text{kJ mol}^{-1} \quad (2)$$

$$ZrO_2 + SiO_2 = ZrSiO_4,\ \Delta G = -3\ \text{kJ mol}^{-1} \quad (3)$$

$$SrO + ZrO_2 = SrZrO_3,\ \Delta G = -19\ \text{kJ mol}^{-1} \quad (4)$$

$$SrSiO_3 + ZrO_2 = SrZrO_3 + SiO_2,\ \Delta G = 51\ \text{kJ mol}^{-1} \quad (5)$$

$$BaSiO_3 + ZrO_2 = BaZrO_3 + SiO_2,\ \Delta G = 97\ \text{kJ mol}^{-1} \quad (6)$$

Clearly, the silicates are mostly favorable to form during crystallization (Eqs. (1) and (2)), and they should be chemically compatible with YSZ electrolyte without forming any zirconates (Eqs. (5) and (6)). There are other possible reaction products between alkaline earth and ZrO_2 besides $SrZrO_3$ (e.g., Sr_2ZrO_4, $Sr_3Zr_2O_7$, and $Sr_4Zr_3O_{10}$); however, these complex compounds all resulted in positive Gibbs free energies, so they would be also deemed less likely to form. No distinct interfacial reaction product was observed at the interface with YSZ, as shown in Figs. 4 and 5 for air side and fuel side (see insert in Fig. 2A for locations), respectively. The microstructure near the YSZ electrolyte (within about 20 microns) did look somewhat different from the matrix and appeared to be porous. This is likely due to differential polishing since YSZ is more stiff and hard than the phases in the glass. No distinct corrosion or glass penetration (e.g., along YSZ grain boundary) was observed on the thin electrolyte. This seems consistent with the simple thermodynamics calculation of Eqs. (4) and (5) in that the formation of $SrZrO_3$ or $BaZrO_3$ was unfavorable. The reaction between SiO_2 and ZrO_2 appeared thermodynamically favored, however, no distinct $ZrSiO_4$ phase was identified along the interface. This is likely due to the low magnitude of the free energy of reaction, causing the SiO_2 to react preferentially with other oxides in fine particle or molecular form in the glass to form crystalline phases. The YSZ electrolyte was already sintered at higher temperature (~1400 °C) and hence the activity would be much lower than other oxides in the glass. It's worthy to note there is fracture near the glass interfaces whether at YSZ electrolyte or the aluminized AISI441 substrate. These fractures are likely caused by metallurgical sample preparation, i.e., cutting, and grinding, due to differences in stiffness and hardness rather than residual stresses since sealing glass YSO77 has a matching CTE with mating materials.

The glass microstructure was similar for both the air side and the fuel side, with a uniformly distributed rod-shaped dark phase and irregular shaped white phase in between. This is the same as the glass in the central section of the seal (Fig. 2), away from either end. In the previous section, EDS analysis showed the dark rod-shaped phase had a (Sr,Ba)/Si ratio close to 1 and was likely to be a solid solution of $SrSiO_3$ and $BaSiO_3$. This appeared to be consistent

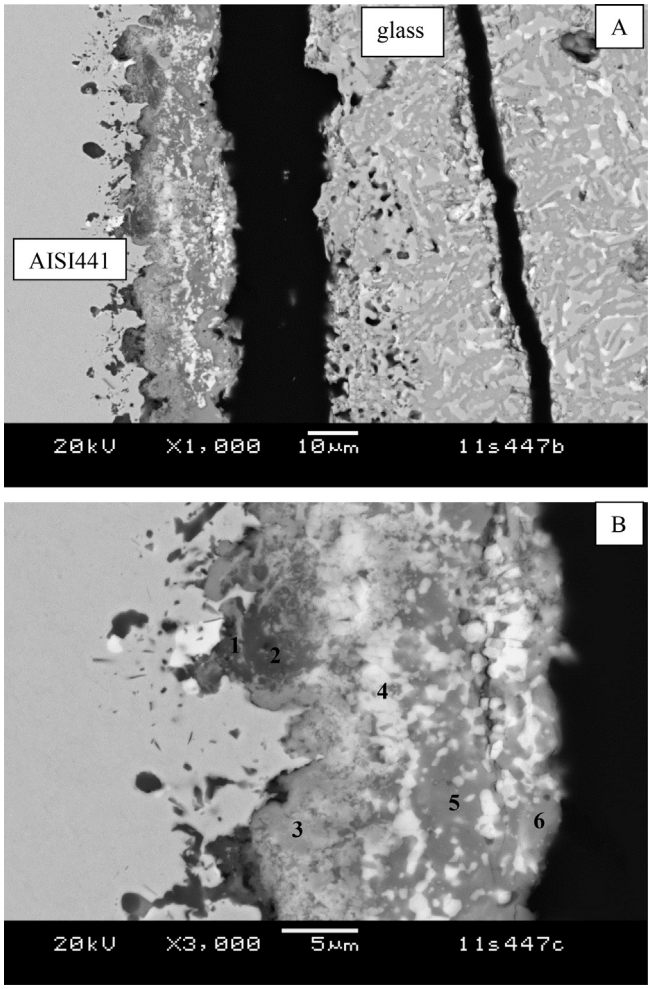

Fig. 7. Microstructure of the refractory sealing glass at the aluminized AISI441 interface near air side, (A) low magnification shows the glass and aluminized AISI441, (B) higher magnification of the circled region in (A). The chemical analysis of spots (#1–#6 in B) is listed in Table 4.

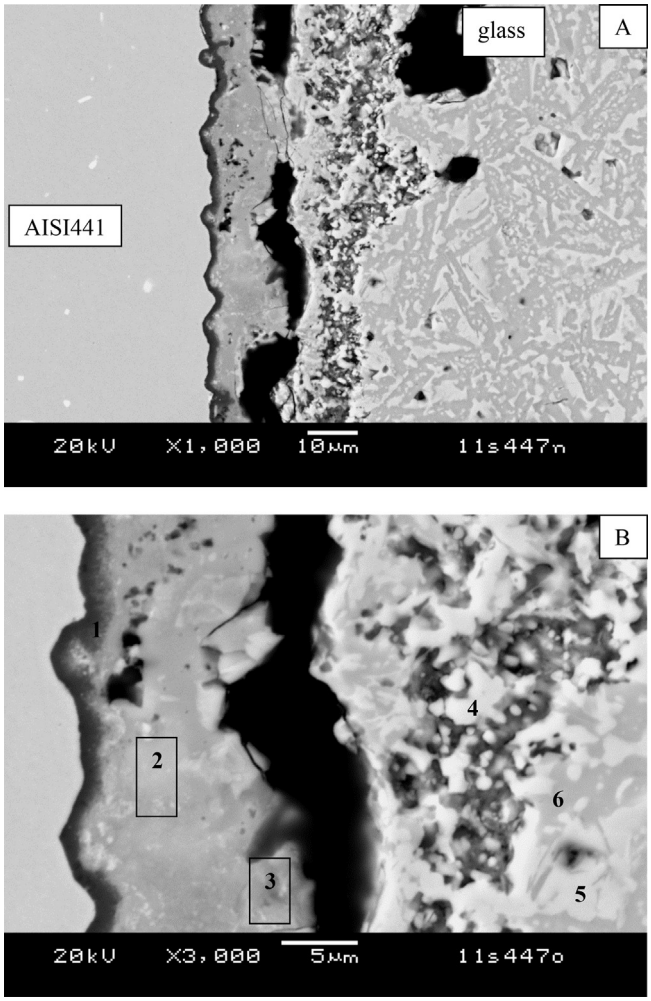

Fig. 8. Microstructure of the refractory sealing glass at the aluminized AISI441 interface near fuel side, (A) low magnification shows the glass and aluminized AISI441, (B) higher magnification of the circled region in (A). The chemical analysis of spots (#1–#6 in B) is listed in Table 5.

with thermodynamics calculation of the stability of Sr–Si–O system which showed $SrSiO_3$ to be stable in both oxidizing and reducing environments at 800 °C, as shown in Fig. 6 (using the same HSC software). In terms of microstructure stability, the glass near the air and fuel side showed similar pore morphology and sizes to those observed in the central section where the glass was shielded from these environments. No large pore formation or abnormal grain growth was identified. Selected spots within this region were analyzed with EDS; the results are listed in Tables 2 and 3, for Figs. 4B and 5B, respectively. No traces of glass constituents were identified within the YSZ electrolyte (area #1 Table 3), and only a minimal amount of Zr was detected a few microns away from the glass/YSZ interfaces (spot #4 Table 2, and spot #3 Table 3). Sulfur was detected in small concentrations within the darker phases (spot #2 Fig. 4B and spot #3 Fig. 5B), and was attributed to trapped polishing media.

3.3. Refractory sealing glass at aluminized AISI441 interface

Sealing glass at the aluminized AISI441 interface was also characterized. Typical microstructures are shown in Figs. 7 and 8 for the air side and fuel side, respectively. EDS analysis of selected spots as shown in Figs. 7B and 8B are listed in Tables 4 and 5, respectively. At both the air and fuel side, there was a featureless region of ~5–10 microns near the interface (Figs. 7B and 8B) as compared to the glass matrix of intertwined and well distributed phases (Figs. 7A and 8A). The presence of Al (low atomic number) also made this region darker than the glass matrix. The corrosion of glass on the protective alumina coating seemed to be more severe at the air side than the fuel side in that the coating was no longer continuous on the air side as compared to the fuel side (spot #1 in Fig. 8B, about 1 μm thick). In addition, Al diffused farther at the air side than the fuel side. For example, the Al concentration was detected to be ~14 at% at ~20 μm from the air-side interface (spot #6 in Fig. 7B), but was only ~8 at% at ~15 μm from the fuel-side interface (area #3 in Fig. 8B). The corrosion of the alumina layer also resulted in the outward diffusion of metal species (Cr, Fe, and Mn), and, in particular, a high concentration of Cr. However, no distinct evidence of $SrCrO_4$ or $BaCrO_4$ formation was identified within this region at the air side where the formation of these chromates is thermodynamically favored and often observed [9,20].

No distinct or large precipitates/crystallites were found within the featureless region near the interface on either the air and fuel side. A stable crystalline phase of celsian ($BaAl_2Si_2O_8$) was commonly observed in the alkaline-earth aluminosilicate glasses [6]. This crystalline phase was deemed undesirable due to low CTE, and the initially formed meta-stable hexagonal phase (CTE of $\sim 8 \times 10^{-6}$ ppm/°C) can gradually transform during operation into the more stable monoclinic phase with a very low CTE of $\sim 3 \times 10^{-6}$ ppm/°C. Sr can form a similar $SrAl_2Si_2O_8$ celsian phase which would be expected to have a similar low CTE, although no published data was available. The spot analysis in Fig. 7B (#2–#6 in Table 4) seemed to indicate no celsian phase formation in this region. Thermodynamic calculations of possible reactions of major glass constituents with Al_2O_3 at 800 °C are listed below:

$$SrSiO_3 + SiO_2 + Al_2O_3 = SrAl_2Si_2O_8,\ \Delta G = -59\ \text{kJ mol}^{-1} \quad (7)$$

$$BaSiO_3 + SiO_2 + Al_2O_3 = BaAl_2Si_2O_8,\ \Delta G = -64\ \text{kJ mol}^{-1} \quad (8)$$

$$SrO + 2SiO_2 + Al_2O_3 = SrAl_2Si_2O_8,\ \Delta G = -191\ \text{kJ mol}^{-1} \quad (9)$$

$$BaO + 2SiO_2 + Al_2O_3 = BaAl_2Si_2O_8,\ \Delta G = -225\ \text{kJ mol}^{-1} \quad (10)$$

The formation of a Sr-celsian phase was thermodynamically favorable, but was kinetically less likely due to the more complex

Table 4
Chemical analysis of spots#1–#6 in Fig. 7B.

Spot#	O	Na	Al	Si	Ti	Cr	Mn	Fe	Sr	Nb	Ce	Ba
1	66.74	0.76	26.89	0.94	0.83	1.35	0.12	0.41	1.48	0.47		
2	62.68	0.59	32.13	0.65	0.85	1.63	0.12	0.17	1.17			
3	71.71		2.46		4.81	10.51	5.41	0.36	4.05		0.46	
4	67.52	0.74	2.11			14.01	1.08	0.26	3.31			10.97
5	61.55	5.25	14.38	5.82		4.13			7.17			1.49
6	63.91	3.83	13.99	3.86	0.41	3.05	1.55	0.35	8.25			0.61

Table 5
Chemical analysis of spots#1–#6 in Fig. 8B.

Spot#	O	Al	Si	Cr	Mn	Fe	Sr	Y	Ba
1	62.29	31.45		1.51		4.58			0.18
2	63.44	14.01	5.38	4.76	0.32	2.48	3.47	0.43	5.71
3	64.79	8.23	4.53	4.57	0.25	2.58	10.72	1.62	2.72
4	68.62	1.12	7.31	0.13		0.74	12.07	8.46	1.54
5	69.27		5.31				12.13	11.36	1.94
6	63.40		19.43				15.82		1.35

structure of $SrAl_2Si_2O_8$ compared to $SrSiO_3$ and the presence of other cations like Cr, Ti, and Mn. The formation of $BaAl_2Si_2O_8$ was even more thermodynamically favorable (due to even more negative Gibbs energy); however, the total amount of Ba in the glass was small (6 mol%) and was expected of less significance than Sr (42.5 mol%).

3.4. Sealing glass volatility

In addition to the chemical compatibility with mating materials, the sealing glass also needs to demonstrate microstructural stability. The current sealing glass YSO77 appeared to meet these requirements without exhibiting abnormal grain growth or formation of large voids/defects. One other concern, especially for stationary applications where 40,000 h of life is expected, is the potential material loss due to volatility. The oxide sealing glasses after crystallization are typically more thermally stable than the parent glass, especially in the oxidizing environment. The crystalline phases tend to have higher melting point than the parent glass. For example, the main crystalline phase of $SrSiO_3$ has a melting point of ~1580 °C [21] and the melting point of the minor phase Ca_2SiO_4 is ~2130 °C [22], The initial glass was melted at ~1400 °C and the as-made glass had a softening point of 705 °C. However, these materials may form volatile species in the presence of water vapor at elevated temperatures, thereby reducing the upper operation temperatures for these oxides. For example, thermal stability of simple oxides such as SiO_2, Al_2O_3, and Cr_2O_3 has been investigated in a high-temperature water vapor environment [23,24]. Opila et al. determined that the approximate upper use temperature for SiO_2 decreased from 1575 °C in ambient air (1% H_2O) to 1370 °C in humid air (10 vol.% H_2O at 1 atm), and to 967 °C in humid, pressurized air (10 vol.% H_2O at 10 atm); at these temperatures, the partial pressure of all volatile species was equal to 1×10^{-7} MPa. In our long-term test, no volatile species were collected and analyzed; however, possible vapor species such as $B_3H_3O_6$, SiO, $Si(OH)_4$, $Sr(OH)_2$, and $Ba(OH)_2$, and $Ca(OH)_2$ were proposed [23,25]. A very similar refractory glass YSO75 was tested for volatility at 800 °C under flowing wet reducing gas (30% H_2O and 70% of 2.75% H_2/Ar) for ~1600 h. Glass YSO75 had the same particle size (#100 mesh) and sintered with the same temperature profile as glass YSO77. The normalized weight loss versus time is plotted in Fig. 9. Clearly, there appeared to be two stages of weight loss. The first stage, up to ~600 h, showed a more linear behavior than the second stage (from ~600 h until ~1600 h). The estimated weight loss rate was $\sim 3.3 \times 10^{-7}$ g cm^{-2} h and $\sim 3.6 \times 10^{-8}$ g cm^{-2} h for the first and second stage, respectively. The volatility rate of a borate glass (#59) Sr (20%)–Ba (20%)–B (20%)–Si (40%) in wet (30% H_2O) reducing gas (10% H_2/N_2) was determined to be $\sim 5.5 \times 10^{-6}$ g cm^{-2} h at 780 °C during a 7 days run [25]. The weight loss was attributed to the volatile species of $B_3H_3O_6$(g) [25], and the higher rate was likely due to a much higher B_2O_3 content as compared to 8.5 mol% in glass YSO75. It was suspected that as the B_2O_3 in the outer exposed surface was gradually lost as volatile species, B_2O_3 inside the glass matrix surrounded by the crystalline phases had less exposed surface area to react with water vapor. Hence the weight loss rate was greatly reduced. It should also be noted that oxide glasses tend to have different volatile species and lower weight loss in an oxidizing environment than in wet and reducing gases. For example Zhang et al. reported a weight loss rate by BO_2(g) of $\sim 8.8 \times 10^{-7}$ g cm^{-2} h in dry air as compared to $\sim 5.5 \times 10^{-6}$ g cm^{-2} h in wet reducing gas at 780 °C for glass #59 [25]. The volatility of glass YSO75 in an oxidizing environment was therefore not measured.

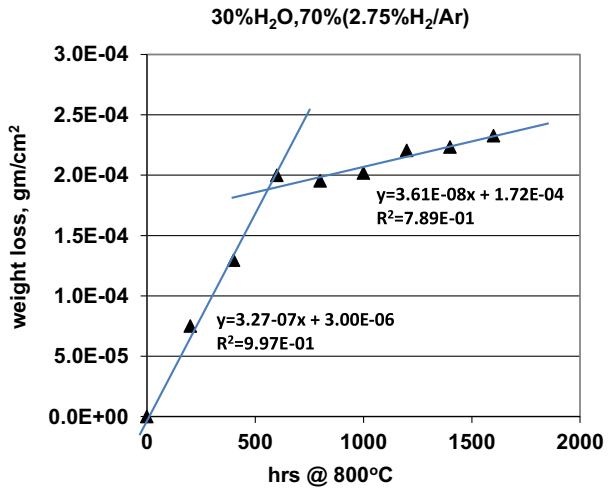

Fig. 9. Volatility study of glass YSO75 at 800 °C in flowing wet (30 vol.% H_2O) reducing gas. The steady-state volatility rate was determined using data after the initial (~600 h) aging.

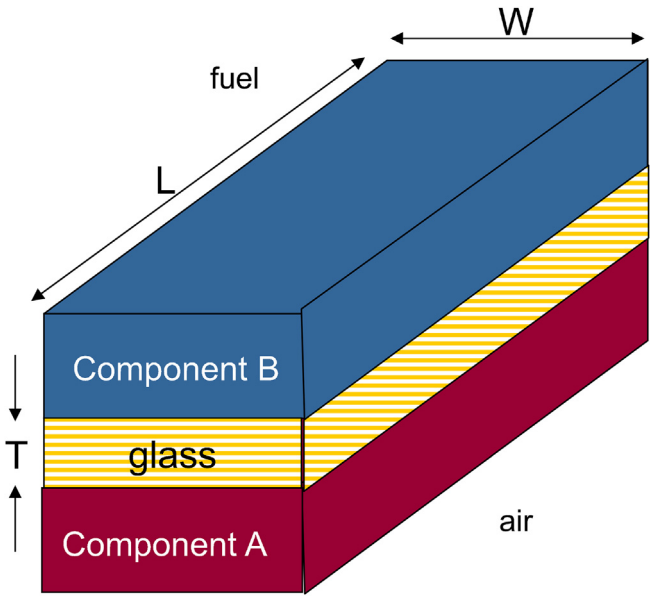

Fig. 10. Schematic drawing showing the generic geometry of a sealing glass and two mating SOFC components used for estimating the material loss. The glass after sealing has dimensions of *T*, *L*, and *W*.

To assess the material loss issue for long-term operation, a generic geometry of sealing glass with mating materials was evaluated, as shown schematically in Fig. 10. The sealing glass has a sealing width of *W*, sealing length *L* and thickness of *T*. One can estimate the material loss during the 40,000 h operation as:

$$\text{Total fractional material loss} = 40000ATL/(\rho WTL) = 40000A/(\rho W) \quad (11)$$

where A is the volatility rate (3.6×10^{-8} g cm^{-2} h), ρ is the density of the glass (3.5 g/cc). Thus, while the absolute material loss (40,000ATL) depends on the exposed surface area (TL), the fractional material loss is inversely proportional to the width of the sealing glass, and independent of length and thickness of the glass. Using a typical sealing width of 5 mm, the calculated total weight loss is 0.082%. This would not be expected to have a significant effect on the integrity of the sealing glass.

4. Summary and conclusion

A generic solid oxide fuel cell stack test fixture was developed to evaluate candidate materials and processing under realistic conditions. Part I of the work addressed the stack fixture, seal system and cell performance of a 3-cell short stack at 800 °C for 6000 h. Part II of the work examined the sealing glass stability, microstructure development, and interfacial reactions with both YSZ electrolyte and aluminized AISI441 interconnect. The refractory glass YSO77 (Ba–Sr–Y–B–Si) showed the desired chemical compatibility with YSZ electrolyte in that no discernable interfacial reaction was identified, consistent with thermodynamic calculations. The glass also showed no penetration into the thin electrolyte. At the aluminized AISI441 interface, the protective alumina coating appeared to be corroded by the sealing glass, and the air side showed more attack than the fuel side. Metal species such as Cr, Mn, and Fe were detected at the vicinity of the interface; however, no chromates were found at the air side. Volatility was also studied in a similar glass and weight loss in a wet reducing environment was determined. Using the steady-state volatility data, the life time (40,000 h) weight loss of refractory sealing glass YSO77 was estimated to be less than 0.1 wt%. Overall, the refractory sealing glass YSO77 proved to be a viable candidate for SOFC sealing applications.

Acknowledgments

The authors would like to thank S. Carlson for SEM sample preparation, and J. Coleman for SEM analysis. This work summarized in this paper was funded by the US Department of Energy's Solid-State Energy Conversion Alliance (SECA) Core Technology Program. The authors would like to thank Shailesh Vora, Briggs White, Patcharin Burke, and Joe Stoffa from NETL for helpful discussions. Pacific Northwest National Laboratory is operated by Battelle Memorial Institute for the US Department of Energy under Contract no. DE-AC06-76RLO 1830.

References

[1] N.Q. Minh, J. Am. Ceram. Soc. 76 (3) (1993) 563–588.
[2] B.C.H. Steele, J. Mater. Sci. 36 (2001) 1053–1068.
[3] S.C. Singhal, in: S.C. Singhal, M. Dokiya (Eds.), Solid Oxide Fuel Cells (SOFC VI) Proceedings of the Sixth International Symposium, The Electrochemical Society, Proceedings, vol. 99-19, 1999, pp. 39–51.
[4] R. Bolden, K. Foger, T. Pham, in: S.C. Singhal, M. Dokiya (Eds.), Solid Oxide Fuel Cells (SOFC VI) Proceedings of the Sixth International Symposium, The Electrochemical Society, Proceedings, vol. 99-19, 1999, pp. 80–87.
[5] A. Khandkar, S. Elangovan, J. Hartvigsen, D. Rowley, R. Privette, M. Tharp, in: S.C. Singhal, M. Dokiya (Eds.), Solid Oxide Fuel Cells (SOFC VI) Proceedings of the Sixth International Symposium, The Electrochemical Society, Proceedings, vol. 99-19, 1999, pp. 88–94.
[6] K.D. Meinhardt, D.-S. Kim, Y.-S. Chou, K.S. Weil, J. Power Sources 182 (1) (2008) 188–196.
[7] Y.-S. Chou, E.C. Thomsen, R.T. Williams, J.-P. Choi, N.L. Canfield, J.F. Bonnett, J.W. Stevenson, A. Shyam, E. Lara-Curzio, J. Power Sources 196 (5) (2011) 2709–2716.
[8] Y.-S. Chou, J.W. Stevenson, P. Singh, J. Electrochem. Soc. 154 (7) (2007) B644–B651.
[9] Z. Yang, K.D. Meinhardt, J.W. Stevenson, J. Electrochem. Soc. 150 (8) (2003) A1095–A1101.
[10] Y.-S. Chou, J.W. Stevenson, P. Singh, J. Power Sources 185 (2) (2008) 1001–1008.
[11] S.P. Simner, M.D. Anderson, G.-G. Xia, Z. Yang, L.R. Pederson, J.W. Stevenson, J. Electrochem. Soc. 152 (4) (2005) A740–A745.
[12] H. Yokokawa, T. Horita, N. Sakai, K. Yamaji, M.E. Brito, Y.-P. Xiong, H. Kishimoto, Solid State Ionics 177 (7) (2006) 3193–3198.
[13] S. Taniguchi, M. Kadowaki, H. Kawamura, T. Yasuo, Y. Akiyama, Y. Miyake, T. Saitoh, J. Power Sources 55 (1) (1995) 73–79.
[14] Y.D. Zhen, A.I. Tok, S.P. Jiang, F.Y.C. Boey, J. Power Sources 170 (1) (2007) 61–66.
[15] K. Fujita, K. Ogasawara, Y. Matsuzaki, T. Sakurai, J. Power Sources 131 (2) (2004) 261–269.
[16] T. Komatsu, R. Chiba, H. Arai, K. Sato, J. Power Sources 176 (1) (2008) 132–137.
[17] Z. Yang, G. Xia, Z. Nie, J. Templeton, J.W. Stevenson, Electrochem. Solid State Lett. 11 (8) (2008) B140–B143.
[18] J.-P. Choi, K. Scott Weil, Y.-S. Chou, J.W. Stevenson, Z.-G. Yang, Int. J. Hydrogen Energy 36 (7) (2011) 4549–4556.
[19] Y.-S. Chou, J.W. Stevenson, J.-P. Choi, J. Power Sources (2013) in press.
[20] T. Zhang, R.K. Brow, W.G. Fahrenholtz, S.T. Reis, J. Power Sources 205 (5) (2012) 301–306.
[21] J.W. Greig, Am. J. Sci. 13 (5) (1927) 19.
[22] B. Phillips, A. Muan, J. Am. Ceram. Soc. 42 (9) (1959) 412–423.
[23] E.J. Opila, N.S. Jacobson, D.L. Myers, E.H. Copland, J. Met. 58 (1) (2011) 22–28.
[24] N.S. Jacobson, D.L. Myers, E.J. Opila, E.H. Copland, J. Phys. Chem. Solid 66 (3) (2005) 471–478.
[25] T. Zhang, W.G. Fahrenholtz, S.T. Reis, R.K. Brow, J. Am. Ceram. Soc. 91 (8) (2008) 2564–2569.